Indian Journal of Biochemistry & Biophysics
Vol. 60, January 2023, pp. 43-54
DOI: 10.56042/ijbb.v60i1.62503

Assessment of YME1L and mitofusin2 as a possible diagnostic and/ or therapeutic target in hepatocellular carcinoma

Nabil Mohie Abdel-Hamid[1], Shimaa A Abass[1]*, Ramadan A Eldomany[2] & Sherin Zakaria[3]

[1]Biochemistry Department; [2]Department of Microbiology and Immunology; [3]Department of Pharmacology and Toxicology, Faculty of Pharmacy, Kafrelsheikh University, Kafrelsheikh-33516, Egypt

Received 21 April 2022; *revised 09 December 2022*

The contribution of mitochondrial dynamics to the development and progression of hepatocellular carcinoma (HCC) remains controversial. Accordingly, the present study tries to illustrate the role of mitochondrial dynamics proteins (mitofusin-2 (*Mfn2*) and YME1L) in hepatocarcinogenesis. Five groups were used: the control group and three HCC groups (after 8, 16, and 24 weeks from DENA induction). The last group was treated with Sorafenib (SP) (10 mg/kg), *via* oral gavage for 4 weeks after cancer induction. This study revealed that *Mfn-2* was downregulated and YME1l was overexpressed in different HCC groups. This dysregulation of mitochondrial dynamics proteins was associated with high hepatic levels of cyclin D1, MMP-9, and MDA and overexpression of ki67 as well as decreasing the hepatic expression of tissue inhibitor of matrix metalloproteinase-3 (*Timp-3*) and *Bax*. To confirm the possible role of *Mfn2* and YME1L in HCC, we assessed the effect of sorafenib on these parameters and its related HCC characteristics. Sorafenib corrected the level of *Mfn2* and YME1L and decreased tumor cell proliferation as well. We also elucidated that mitochondrial dynamics proteins (*Mfn2* and YME1L) could be a good therapeutic target for HCC.

Keywords: HCC biomarker, Matrix metalloproteinase, Mitochondrial dynamics, Mitochondrial fusion, TIMP-3

Hepatocellular carcinoma (HCC) is considered the 6th most frequent tumor and the 4th most prevalent reason for mortality associated with cancer worldwide. The high mortality rate of HCC is due to its late diagnosis and non-satisfactory therapeutic response[1]. HCC diagnosis involves imaging and blood tests besides biopsy, which is also done in some cases for defining the grade and type of HCC and identifying the stage of the tumor[2]. The classification of various cancer types and grades does not depend on a histological investigation alone. So, new approaches are required in the development of novel molecular methods for cancer diagnosis, which would support the histological methods to save time, limit human errors, and solve unclear cases[3]. Particular attention should be directed to the molecular analysis depending on both quantitative and qualitative characteristics of tissues, which always change during tumorigenesis and treatment. This may help in the identification of tumor grades.

Mitochondria are characterized by being highly dynamic as they perform continuous fission and fusion processes. Numerous guanosine triphosphatases (GTPases) control these critical processes[4]. The mitochondrial function is associated with their structure as mitochondrial dynamics participate in several vital processes, including mitophagy, cell death, cell metabolism, and regulation of cell cycle[5]. The fission process is mediated by GTPase dynamin 1-like protein (Drp1) whereas, mitofusins (*Mfn1*, *Mfn2*), and OPA1 mitochondrial dynamin-like GTPase (OPA1) regulate the fusion process[6]. It was reported that the mitochondrial dynamic is shifted from fusion to fission in various tumors including HCC[7].

Mitofusin 2, the outer mitochondrial membrane (OMM) protein, participates in promoting the OMM

*Correspondence:
Phone: +201094569476
E-mail: shimaaali211@yahoo.com, shimaa_abass@pharm.kfs.edu.eg

Abbreviations: AFP, alpha-fetoprotein; ALT, alanine aminotransferases; AST aspartate aminotransferases; ANOVA, One-way analysis of variance; DENA, diethylnitrosamine; Drp1, dynamin 1-like protein; ECL, Western Bright enhanced chemiluminescence; ECM, extracellular matrix; ELISA, Enzyme-linked immunosorbent assay; GSH, reduced glutathione; GTPases, guanosine triphosphatases; HCC, Hepatocellular carcinoma; H&E, Hematoxylin and Eosin; IMM, inner mitochondrial membrane; MDA, malonedialdehyde; MFN2, mitofusin-2; MMP9, matrix metalloproteinase 9; OMM, outer mitochondrial membrane; PB, phenobarbital sodium; RT-PCR, real-time polymerase chain reaction; ROS, reactive oxygen species; SD, standard deviation. SP, Sorafenib; Timp-3, Tissue inhibitor matrix metalloproteinase-3; TEM, Transmission electron microscopy

fusion[8]. It was previously reported that *Mfn2* plays an important role in cell autophagy and apoptosis[9]. The expression of *Mfn2* was found to be downregulated in several cancers like colorectal and breast cancers[10,11]. The role of *Mfn2* in the staging of HCC has not been studied yet.

The dynamin-like GTPase OPA1 participates in the control of OMM fusion and mitochondrial structure[6]. Its activity is modulated by proteolytic processing as it presents in two forms: short and long OPA1 (S-OPA1 and L-OPA1). L-OPA1 is hydrolyzed into S-OPA1 with the help of two proteolytic enzymes (OMA1 and YME1L (I-AAA proteolytic enzyme)). Inner membrane-anchored L-OPA1 regulates intimal fusion, whereas, S-OPA1 exists in the membrane space and promotes mitochondrial fission and fragmentation[12]. Inner mitochondrial ATPases associated with diverse cellular activities (AAA) protease (YME1L) are found to regulate different processes including, respiratory chain biogenesis, quality control, and mitochondrial dynamics regulation[13]. Hence, alterations in the YME1L activity could alter the proteostasis of the mitochondrial inner membrane, which results in pathologic mitochondrial dysfunction leading to different human diseases[14]. As the role of YME1L in HCC has not been reported yet; our study was performed to assess the possible role of YMEIL and *Mfn2* in the diagnosis and treatment of HCC in different stages by illustrating their role in tumorigenesis and metastasis.

Material and Methods

Chemicals

Phenobarbital sodium (PB) was purchased from Alpha Chemika (Maharashtra, India), while Diethylnitrosamine (DENA) and sorafenib (Sb) were purchased from Toronto Research Chemicals (Toronto, Canada). Other used chemicals were of high-quality and grade.

Chemicals preparation

For obtaining a suitable volume for injection, 0.9 mL DENA stock solution of concentration 1 mg/mL was dissolved in 12 mL saline to obtain a working DENA solution having a final concentration of 75 mg/mL. On the other hand, 0.5 g PB was dissolved in 1 L of drinking water every day for preparing a 0.05% PB solution. Sorafenib suspension was obtained by suspending 50 mg of sorafenib in 1% CMC (10 mL) for obtaining a final working suspension (5 mg/mL) suitable for oral gavage.

Experimental design

Thirty adult male albino rats having a weight ranging from 110 to 120 g were used. All standard hygienic conditions were provided for the animals including, a well-ventilated room, temperature of 21-25°C, humidity at 55±5%, and 12 h light-dark regime. They were also provided with an appropriate pellet diet and tap water *ad libitum*.

Rats were kept for acclimatization in suitable cages for 7 days. Then they were randomly divided into five groups (6 rats/group):

- **The Control group**: Animals were administrated saline (0.5-0.7 mL, single dose). After 20 weeks from saline administration, they were administrated (0.2-0.7mL) of 1% CMC orally for successive 28 days.
- **The 8 weeks group**: Animals were administrated DENA (200 mg/kg, single intraperitoneal dose). After 14 days of DENA administration, phenobarbital sodium (0.05%) was supplied to their drinking water. Rats were then sacrificed 8 weeks after DENA injection.
- **The 16 weeks group**: Rats were treated as group 3. Rats were sacrificed after 16 weeks of DENA administration.
- **The 24 weeks group**: Rats treated as group II. Rats were sacrificed after 24 weeks of DENA administration.
- **The Sb (10 mg/kg) group**: Rats were administrated *i.p* injection of DENA (200 mg/kg, single dose). Fourteen days after DENA injection, 0.05% phenobarbital sodium was supplied to their drinking water for successive 18 weeks. Sorafenib (10 mg/kg) was administrated *via* oral gavage for further successive 28 days[15] (Fig. 1).

Blood and liver sample collection

Before sample collection, rats were fasted for about 14 h. Diethyl ether was used for anesthetizing rats and blood specimens were then collected through retro-orbital vein puncture using heparinized capillary tubes. Serum samples were then separated by leaving the collected blood specimens for 30 min then centrifuging them at 4°C and 4000 rpm for 15 min. Serum aliquots were then stored at −80°C. Rats were then dissected for gentle removal of their livers.

The excised livers were washed with saline, dried, and divided into 4 parts:

- The first liver part, used for histopathological and immunohistochemical investigation, was kept in a buffered solution of formalin (pH 7.4, 10%).

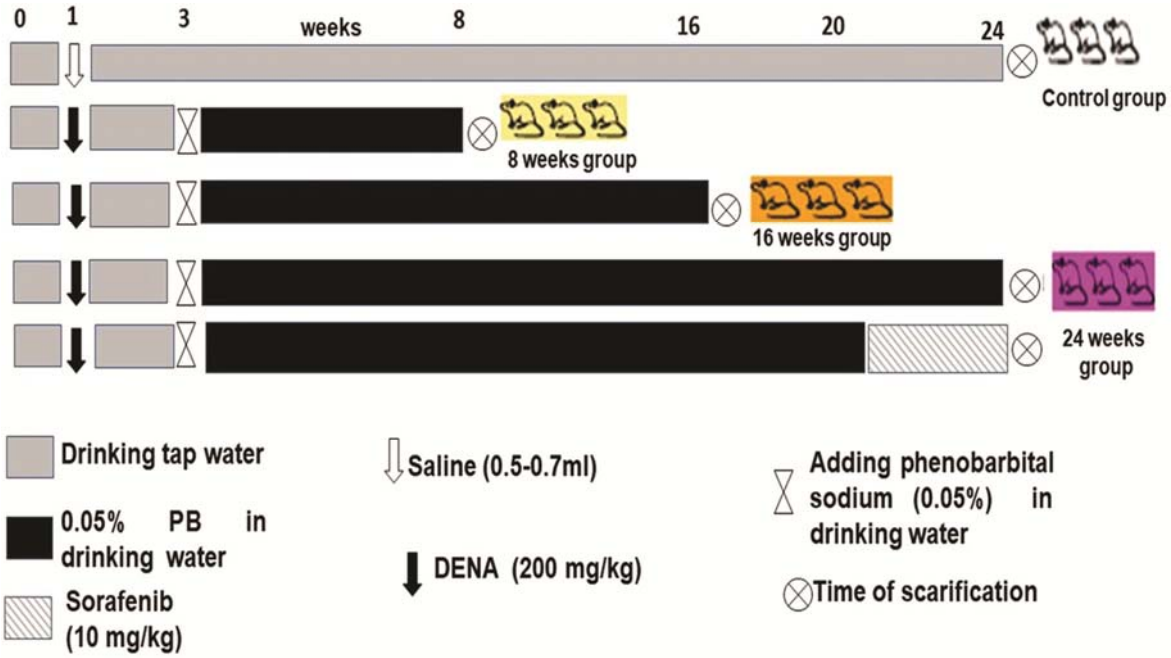

Fig. 1 — Schematic representation of the experimental design. DENA: Diethylnitrosamine. PB: phenobarbital sodium

- The second portion, used for real-time polymerase chain reaction (RT-PCR) investigation, was instantly dipped in RNA later solution and then stored at –80°C.
- The third part was homogenized using RIPA buffer pretreated with protease and phosphatase inhibitors. Centrifugation was then performed to the homogenate at 4°C and 5000 rpm for 15 min. The obtained supernatant was then sucked and kept at –80°C.
- The fourth part containing small liver samples (1 mm thickness) was immediately fixed by dipping liver samples in 4F1G solution (4% Formaldehyde and 1% Glutaraldehyde, pH= 7.2) and stored at 4°C for using them in the transmission electron microscopy (TEM) investigation.

Histopathological and immunohistochemical investigation of liver tissues

Liver tissues stored in the buffered formalin solution were washed and dehydrated by ethanol of different serial ascending dilutions. Paraffin wax blocks were then formed by embedding the liver tissues in the wax at 60°C for 24 h. The blocks were cut into thin sections (5 µM thickness) and deparaffinized. Hematoxylin and Eosin stain (H&E) was then used for staining liver sections, which were then examined using a suitable light microscope.

Immunohistochemical investigation of ki67 was performed on the thin liver sections, which were deparaffinized and rehydrated. Endogenous peroxidase was blocked using Hydrogen peroxide (3%). On the other hand, liver sections were treated with 1% bovine serum albumin for blocking non-specific binding sites. Liver sections were immunostained using Anti-rat ki67 monoclonal antibody (1:200 dilution, Abcam Inc., USA). Horseradish peroxidase was used as a secondary antibody. A chromogen (2% 3,3 diaminobenzidine solution) was then used and the slides were counterstained using H&E. The staining intensity was then evaluated and the percentage of positive cells per 1000 hepatic cells was then calculated.

Assessment of biochemical parameters

The activities of alanine and aspartate aminotransferases (ALT, AST) were calorimetrically assessed in serum specimens using commercially available kits (Biodiagnostic Company, Egypt)[16].

The liver homogenate samples were used for the spectrophotometric measurement of the hepatic contents of malondialdehyde (MDA) and reduced glutathione (GSH) (Biodiagnostic Company, Egypt) based on standard methods[17] and[18], respectively.

The Enzyme-linked immunosorbent assay (ELISA)

Serum samples were used for the estimation of the alpha-fetoprotein (AFP) concentration, the hepatic matrix metalloproteinase 9 (MMP 9), and the hepatic

cyclin D1 (MyBioSource, USA) using The ELISA technique.

Real-time polymerase chain reaction analysis (RT-PCR)

Hepatic *Mnf2*, *Timp-3*, and *Bax* gene expressions were measured using the RT-PCR technique. TRIzol reagent (Thermo Fisher, USA) was used for total RNA isolation from hepatic tissue samples. A Quanti Nova SYBR Green (QIAGEN, Germany) was used for the determination of the quantities of RNA amount/sample. Single-stranded complementary DNA (cDNA) was obtained from reverse-transcription of 1 µg total RNA using a high-capacity C-DNA reverse transcription kit (Thermo Fisher, USA). The used internal control reference was rat β-actin (housekeeping gene). The primer sequences were designed as the following:

Mfn-2: F:5′CGGCGAATTGGAGATGAACTGG3′, R:5′CTAGCAAAGTAGAAGAGGGCAACC3′
Timp-3: F: 5′-GCCTTCTGCAACTCCGACATC-3′, R: 5′-CGTGTACATCTTGCCATCATA-3′
Bax: F: 5′CGGCGAATTGGAGATGAACTGG3′, R:5′CTAGCAAAGTAGAAGAGGGCAACC3′ and **β-actin**: F:5′-GATGGTGGGTATGGGTCAGAAGGAC-3′, R:5′-GCTCATTGCCGATAGTGA-TGACT-3′.

The PCR protocol was used under the following conditions: incubation for 5 min at 95°C followed by incubation at 94°C for 20 sec and at 60°C for 1 min (40 cycles). The identity and specificity of RT-PCR products were detected by using melting curve analysis. The relative gene expressions of *Timp-3*, *Mnf2*, and *Bax*/ β-actin in liver samples were obtained using the $2\text{-}\Delta\Delta^{Ct}$ method.

Western blotting assay

RIPA lysis buffer (Thermo Fisher, USA) treated with a cocktail of proteinase and phosphatase inhibitors (Sigma-Aldrich) was used for preparing liver homogenate samples. Calculated volumes of liver homogenate specimens having 30 µg total protein concentration were separated using SDS-PAGE gel (12%). The nitrocellulose membrane was blocked using 3% bovine serum albumin and used as solid support for proteins that were transferred into it. The membrane was then incubated with the YME1L primary antibodies (dilution 1: 1000, ABclonal company, USA) for 12 h at 4°C and then incubated with diluted a secondary antibody at room temperature (25°C) for 1 h.

The membrane was then visualized using Western Bright enhanced chemiluminescence (ECL) HRP Substrate and the intensity of the estimated protein bands was then calculated using Image analysis software (ImageJ). The YME1L protein expression was calculated and normalized to β-actin.

Transmission electron microscopy (TEM)

Animal livers were cut into small pieces, which were immediately fixed using 4F1G and stored at 4°C. Osmium tetroxide (OsO4, 2% in phosphate buffer solution) was used for fixation of liver samples for 2 h at 4°C. Subsequently, specimens were rinsed using the buffer, dehydrated by serial acetone concentrations at 4°C. Beam capsules were formed by embedding the specimens in resin and backing them in an oven for 48 h at 60°C. Specimens were sliced into 90 nm thickness sections and stained using uranyl acetate (5 min) followed by lead citrate (2 min). The electron microscope was then used for examining liver sections. Mitochondrial length quantification of TEM images was calculated using ImageJ software per cell (Seven cells/ group)[19].

Statistical analysis

The obtained data in this study were analyzed using GraphPad Prism Software version 8.0. (San Diego, CA). They were represented as mean ± standard deviation (SD). One-way analysis of variance (ANOVA) was used for the determination of the variation among different animal groups and the multiple comparisons were done based on the Tukey's-HSD multiple range post hoc test. Fisher's exact test was used for analyzing the Ki67 data. The statistical significance was expressed at $P < 0.05$.

Results

Liver enzymes activities

Our study illustrated that the ALT activity was markedly elevated in the three different HCC stages (8, 16, and 24 weeks), in contrast to the control group with a percentage of change (23.1%, 61.85%, and 137.33%, respectively). It was noticed also that the treatment of sorafenib caused a marked increase in the hepatic ALT activity, in comparison with the control group. The ALT activity significantly increased in the 24 weeks group more than in the16 weeks group and it was markedly elevated in the 16 weeks group more than in the 8 weeks group. However, there was no significant change between the hepatic ALT activity in the sorafenib group and the 24-week group (Table 1).

Table 1 — variations in the serum activities of alanine aminotransferase (ALT), and aspartate aminotransferase (AST), serum concentration of alpha-fetoprotein (AFP), and the hepatic content of malonaldehyde (MDA) and reduced glutathione among different stages of hepatocellular carcinoma (HCC) groups, compared to the control group

	ALT (U/L)	AST (U/L)	AFP (ng/mL)	MDA (nmol/g tissue used)	GSH (mmol/g tissue used)
Control	24.64 ± 2.12	24.06± 2.23	4.550±0.38	21.69±2.05	11.55±1.15
HCC (8 weeks)	30.34 ± 2.07*	58.44± 4.7*	10.12±0.99***	56.97±1.53*	5.37±0.54*
HCC (16 weeks)	39.88±4.11$^{*\#}$	71.43±5.6$^{*\#}$	11.88±1.01$^{*\#}$	75.82±6.9$^{*\#}$	3.7±0.38$^{*\#}$
HCC (24 weeks)	58.48±4.27$^{*\#\$}$	78.85±4.56$^{*\#\$}$	14.70±1.39$^{*\#\$}$	85.17±8.97$^{*\#\$}$	2.1±0.2$^{*\#\$}$
Sb (10 mg/kg)	56.06±4.601$^{*\#\$}$	76.85±4.7$^{*\#\$}$	5.537±0.53$^{\#\$\&}$	27.40±2.742$^{\#\$\&}$	8.032±0.5$^{*\#\$\&}$

Data were compared using the Tukey's-HSD multiple range post hoc test and they were expressed as mean ± SD. N=6. *, #, $,and & represent the significant difference against the control group, the 8-week group, the 16-week group, and the sorafenib (Sb) group at P <0.05

In parallel, the AST activity was also markedly increased in the three different stages of HCC (8, 16, and 24 weeks), in contrast to the control group with a percentage of change (+142.8%, +196.8%, and +227.5%, respectively). The sorafenib group also caused a marked elevation in the hepatic concentration of AST, in comparison with the control group. The 24 weeks group markedly elevated the AST activity more than the 16 weeks group, which also exhibited a marked increase in the serum AST concentration more than the 8 weeks group. However, the sorafenib group showed no significant difference in the AST concentration relative to the 24 weeks group (Table 1).

Oxidative stress and antioxidant parameter

Our study revealed that the hepatic MDA concentration showed a marked increase in the three different stages of HCC groups (8, 16, and 24 weeks), with a percent change (162.7%, 249.6, and 292.7%, respectively), in contrast to the control group. The hepatic MDA concentration in the 16 weeks group is markedly elevated compared to the 8 weeks group. The 24 weeks group also caused a marked elevation in the hepatic MDA concentration more than the 16 weeks group. However, the treatment with sorafenib caused a restoration of the elevated hepatic level of MDA near the control level (Table 1).

In parallel, the hepatic GSH concentration was markedly decreased in the three different HCC stage groups (8, 16, and 24 weeks), with a percent of change (–53.3%, –67.96%, and –81.8%, respectively), in contrast to the control group. The 24 weeks group displayed a marked decline in the level of GSH in comparison with the 16 weeks group, which also displayed a significant decrease in the hepatic content of GSH in contrast to the 8 weeks group. The treatment with sorafenib showed a marked decline in the HCC-induced elevation of the hepatic GSH level (Table 1).

Assessment of the tumor marker alpha-fetoprotein (AFP)

The present study revealed that serum AFP level is markedly elevated in the three different HCC stage groups (8, 16, and 24 weeks), with a percent of change (122.4, 161.1, and 230.1, respectively), in contrast to the control group. The 24 weeks group exhibited a significant rise in the serum AFP level in comparison with the 16 weeks group, which also displayed a significant increase in the serum AFP level in comparison with the 8 weeks group. The treatment with sorafenib restored the serum AFP concentration to the control level (Table 1).

Liver histopathological study

The control group exhibited normal hepatic tissue with normal hepatocytes (H) revealing small uniform nuclei and granulated cytoplasm around the central vein (CV). The 8 weeks group showed the presence of a preneoplastic nodule (N) the nodules are of clear type displaying cytomegaly, and double nuclei of the hepatocytes (arrowhead). The 16 weeks showed the presence of preneoplastic foci of a clear type having vacuolar features (black arrows), and centrilobular area revealing marked hepatic degeneration and necrosis (arrowheads). The 24 weeks group displayed the presence of preneoplastic nodules. These nodules are clear type (N) and large-sized showing nuclear pyknosis (arrowhead), vacuolation, and cytoplasmic enlargement. The sorafenib group showed very small size preneoplastic nodules with necrotic changes within the center of the clear type neoplastic foci (arrowheads) (Fig. 2).

The transmission electron microscope

The control group displayed cell organelles of normal features. The control group exhibited

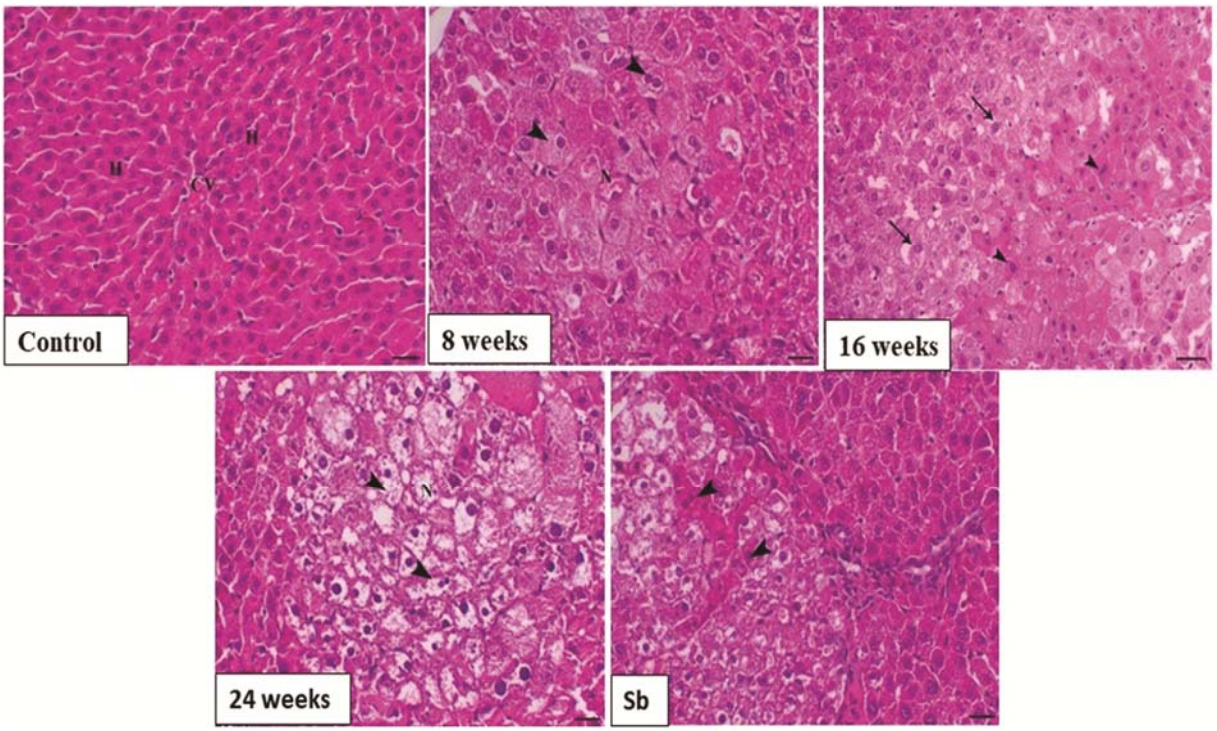

Fig 2 — Representative micrographs of thin sections from liver samples obtained from rats of different studied groups. Bar= 50 µM, H&E, X200

hepatocytes having a large round nucleus containing normal heterochromatin and predominant euchromatin (N). The cytoplasm has multiple round-shaped and small mitochondria (M). Various sites of mitochondrial fusion (arrow) were also noticed. The cells of HCC groups showed numerous nuclei (N) and mitochondria (M) having an irregular membrane (arrow). It was noticed that there were numerous mitochondrial fissions (MF) as constriction of the outer membrane and small mitochondrial fragments. Degenerated mitochondria were noticed to have an inner membrane with disrupted cristes (C) and a detached outer membrane (Fig. 3A). On the other hand, the treatment with sorafenib showed multiple fusion sites of the mitochondria.

The HCC groups of different stages also displayed a marked decline in mitochondrial length, in comparison with the control group. The 24 weeks HCC group caused a marked decline in the length of mitochondria in comparison with the 16 weeks group, which also displayed a marked decline in the mitochondrial length when compared with the 8 weeks group. The sorafenib treatment significantly increased the length of mitochondria in contrast to the different stages of HCC groups (Fig. 3B).

Assessment of the level mitofusin 2 (*Mfn2*) expression

In this study, the hepatic expression of the *Mfn2* gene was markedly declined in the three HCC stages (8 weeks, 16 weeks, and 24 weeks groups), with a percent of change (–40%, –51%, –71%, respectively), in contrast to the control group. The 24 weeks caused a marked decline in the hepatic expression of *Mfn2* in comparison with the 16 weeks group, which also displayed a more marked decline in the hepatic expression of *Mfn2*, in comparison to the 8 weeks group. The treatment with sorafenib exhibited a marked increase in the HCC- induced downregulation of the hepatic *Mfn2* expression (Fig. 3C).

Evaluation of the hepatic expression of YME1L protein

Our study displayed that YME1L was highly expressed in the three different HCC groups (8, 16, and 24 weeks) with a percent change (+304.9%, +379.02%, and +558.5%, respectively), in contrast to the control group. The 24 weeks group markedly increased the hepatic YME1L protein expression in contrast to the 16 weeks group, which also displayed a significant elevation in theYME1L expression in the hepatic tissue comparison to the 8 weeks group. The sorafenib treatment also displayed a marked decline in the HCC- induced elevation of YME1L (Fig. 3D).

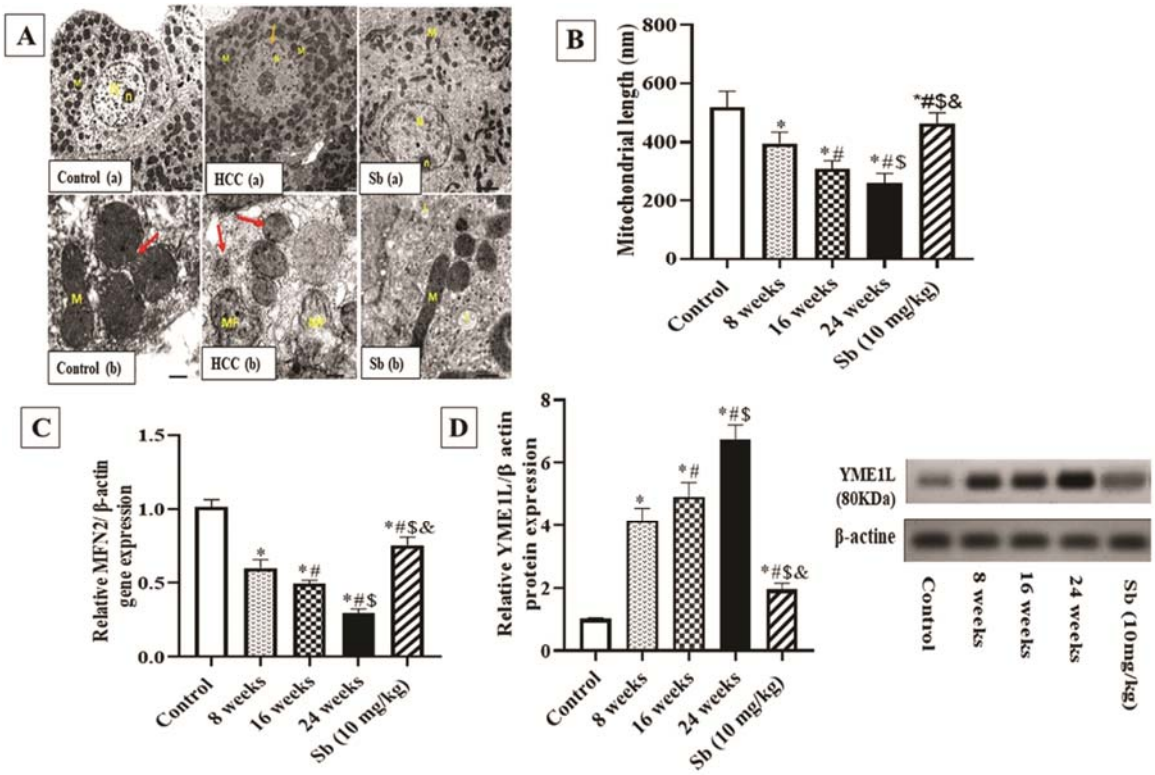

Fig 3— (A) Electron micrograph sections obtained from various studied animal groups. Multiple sites of fusion were observed in the control and sorafenib groups. Controversy, the HCC group showed multiple mitochondrial fission (MF). Bar 500 nm (a) and 200 nm (b);(B) mitochondrial length variations among different groups; (C) The relative gene expression of mitofusin 2 (*Mfn2*) in different animal groups; and (D) The relative protein expression of YME1L in different studied animal groups. Data are expressed as mean ± SD, N= 6. *, #, $, and & represent the significant difference against the control group, the 8-week group, the 16-week group, and the sorafenib (Sb) group at P <0.05

The evaluation of the hepatic *Timp-3* gene and MMP 9 protein expressions

Our study displayed that the hepatic *Timp-3* gene expression was markedly decreased in the three stages of HCC (8, 16, and 24 weeks) with a percent of change (–55%, –59%, and –82.2) in comparison with the control group. The 24 weeks markedly decreased the expression of *Timp-3* in the hepatic tissue in contrast to the 16 weeks group, which also showed a more marked decline in the *Timp-3* expression, in contrast to the 8 weeks group. The sorafenib treatment caused a significant increase in the HCC-induced decline in the *Timp-3* expression in hepatic tissue (Fig. 4A).

In parallel, the hepatic MMP 9 concentration is markedly elevated in the three different HCC stage groups (8, 16, and 24 weeks) with a percent change (+217.1%, +240.4%, and +397.5%, respectively), in contrast to the control group. The 24 weeks group revealed a marked increase in the level of MMP 9 in the hepatic tissue in comparison with the 16 weeks and 8 weeks groups while there is no marked difference in the hepatic MMP 9 level between the 16 weeks and 8 weeks groups. It was noticed that the MMP 9 concentration in the hepatic tissue was markedly decreased in the sorafenib group, compared to the HCC groups (Fig. 4B).

The evaluation of the apoptotic marker *Bax*

Our study exhibited that the *Bax* expression in the hepatic tissue of the three HCC stages (8, 16, and 24 weeks) was significantly decreased with a percent of change (–42%, –51%, and –73%, respectively), contrary to the control group. The 24 weeks group caused a marked decline in the *Bax* gene expression in the hepatic tissue in comparison to the 16-week group, which also displayed a more marked decline than in the 8 weeks group. The treatment with sorafenib displayed a significant rise in the *Bax* expression in contrast to the HCC groups (Fig. 4C).

Evaluation of the cell cycle marker cyclin D 1

The concentration of cyclin D1 in the liver homogenate of the three different HCC stage groups

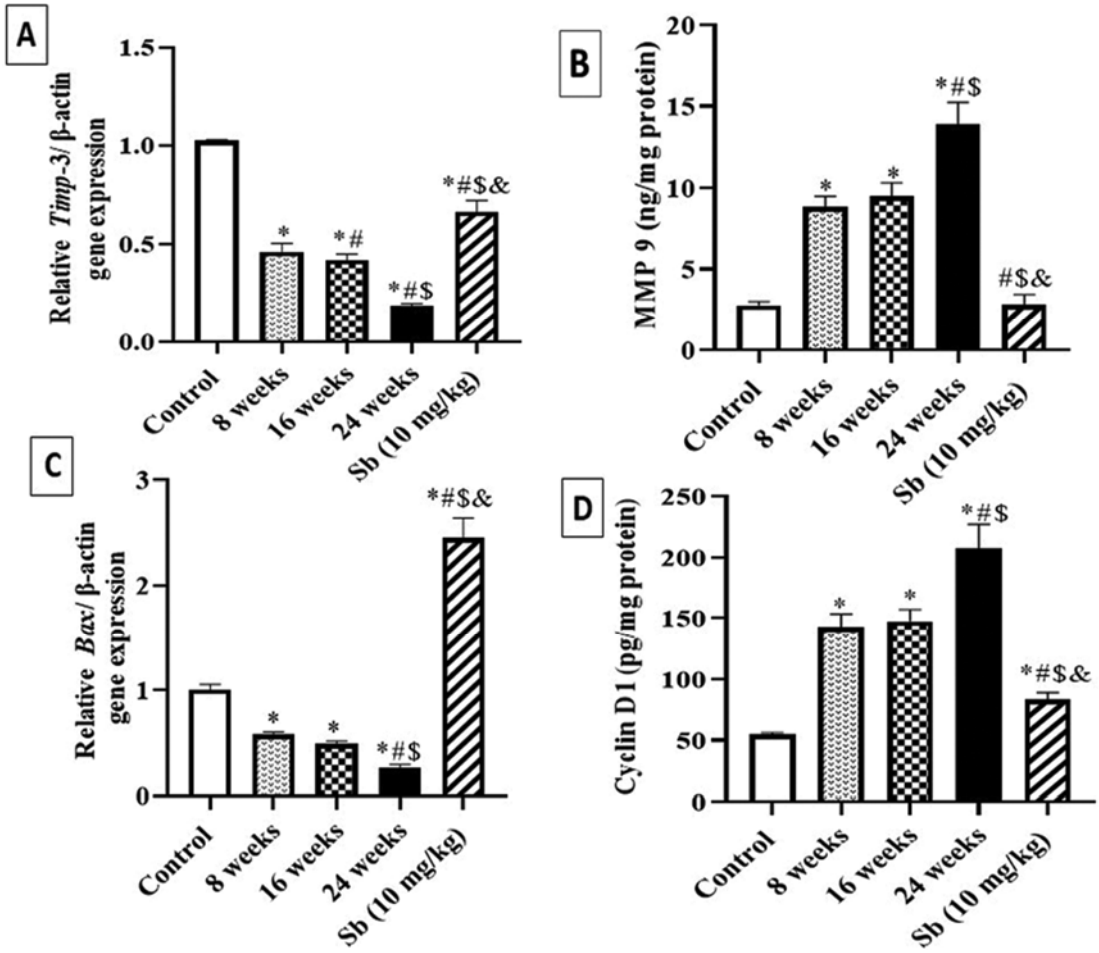

Fig 4 — The relative hepatic expression of (A) tissue inhibitor matrix metalloproteinase (*Timp-3*); (B) matrix metalloproteinase 9 (MMP9); (C) Bax; and (D) cyclin D1 in various animal groups. Data are expressed as mean ± SD. *, #, $, and & represent the significant difference against the control group, the 8-week group, the 16-week group, and the sorafenib (Sb) group at P <0.05. N= 6

(8, 16, and 24 weeks) was markedly increased with percent change (+160.3%, +169.8%, and +279.5%, respectively), in contrast to the control group.

The 24 weeks significantly increased the level of cyclin D1 in the hepatic tissue in contrast to the 16 weeks and the 8 weeks groups, however, the hepatic level of cyclin D1 exhibited no significant change among the 8 weeks and the 16 weeks groups. The sorafenib treatment displayed a marked decline in the cyclin D1 hepatic concentration, in contrast to the HCC groups (Fig. 4D).

The immunohistochemistry results of Ki-67 (cell proliferation marker)

In the present study, the control group revealed a normal hepatic tissue having a limited number of positively stained hepatocytes by the ki-67 antibody. The 8 weeks group showed a positive nuclear expression of ki-67 (brown color) in hepatocytes (black arrows) (22%) that significantly increased in the 16 weeks group (40.4%) and much more increased in the 24 weeks group (87%). The treatment with sorafenib significantly decreased the expression of Ki-67 (17%) in contrast to the different stages of HCC groups (Fig. 5).

Discussion

Despite the advances that have been achieved in the HCC treatment and diagnosis, the HCC mortality rate is increasing rapidly due to late diagnosis and the lack of effective therapy. AFP, the currently used biomarker for HCC diagnosis, possesses poor specificity to detect HCC in all patients, particularly at late stages[20]. Thus, there is an urgent need to identify liver-specific biomarkers for early prediction and proper diagnosis of HCC.

Mitochondria are vital cellular organelles. To meet various cellular requirements, they perform constant

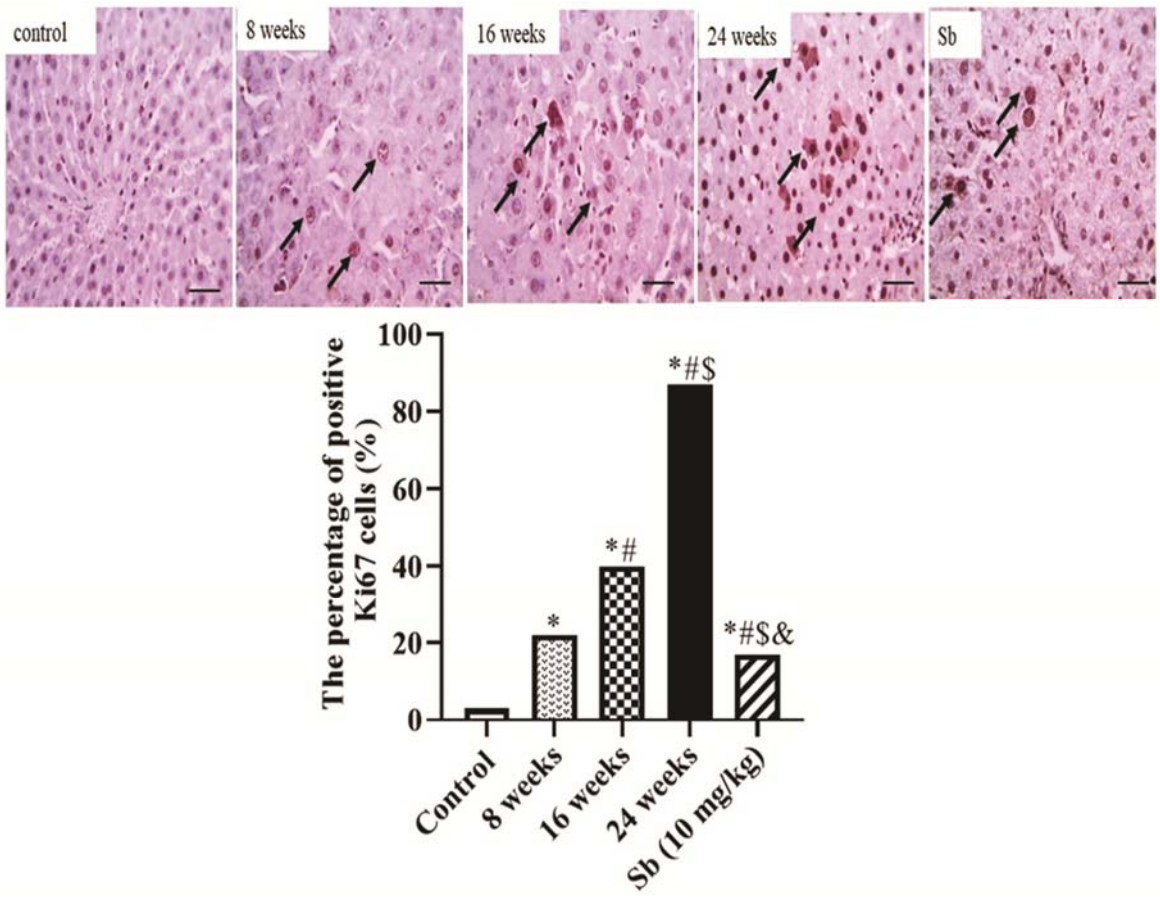

Fig 5 — (A) Microscopic sections from liver samples immunostained against Ki-67. The control group showed negative staining. The hepatocytes of HCC groups showed positive brown nuclear expressions (black arrows) in 8 weeks group that increased in 16 weeks and much more increased in 24 weeks group. Mayer's hematoxylin was used as an IHC counterstain. Bar 50 µm, X:400; and (B) The percentage of hepatic cells positively expressed ki-67 per total 1000 cells in different studied animal groups. Fisher exact test was used for data comparison.*, #, $, and & represent the significant difference against the control group, the 8-week group, the 16-week group, and the sorafenib (Sb) group at P <0.05

fission and fusion dynamics, which are mediated by various lipids and proteins. Dysregulation of mitochondrial dynamics has been associated with the initiation and progression of numerous human cancers, influencing different aspects like cancer stem cell survival, drug resistance, and metastasis[21].

Mitochondrial fission upregulation has been reported to be implicated in the promotion of HCC cells proliferation[22]. Conversely, the role of the opposite process of mitochondrial fission, mitochondrial fusion, in suppressing HCC cells proliferation and metastasis has not been fully illustrated. The mitochondrial fusion process occurs in two steps, including the OMM fusion, which is controlled by mitofusin proteins (*Mfn1*, *Mfn2*), and IMM fusion mediated by OPA1[7,23]. YME1L together with Oma1, inner-membrane peptidases, are responsible for OPA1 processing. Long OPA1 (L-OPA1) is a membrane-bound form of OPA1 that is essential for the fusion of the mitochondrial membrane. Processing of L-OPA1 to short-form impedes the fusion of mitochondrial membrane and may promote fission[24]. Our study tries to illustrate the role of mitochondrial dynamics proteins (YMEIL and *Mfn2*) in HCC diagnosis and being a potential target for HCC therapy like sorafenib.

The present study exhibited that the different HCC groups exhibited multiple mitochondrial fissions in comparison to the control group. These findings agreed with other studies that reported that mitochondrial fission is promoted in HCC and stimulates HCC progression by inducing mt DNA stress[7,25]. It was noticed that the hepatic expression of *Mfn2* and YME1L was significantly altered among

different HCC stages. Where, *Mfn2* is down regulated early after 8 weeks of DENA induction. This effect became more prominent after 16 and 24 weeks of induction. Our finding agreed with a recent study, which also illustrated that *Mfn2* expression was markedly declined in HCC tissues in contrast to paracancerous hepatic tissues[26].

On the other hand, YME1L was upregulated during different stages of HCC. It is significantly increased after 8 weeks of DENA induction. Moreover, it was more upregulated after 24 weeks of DENA induction, compared to 8 and 16 weeks groups. These results refer for the first time to the possible role of these proteins as early markers for HCC diagnosis. However, other studies are required to confirm the possible implication of these proteins as diagnostic and therapeutic targets in other cancers and humans and also to show the relation of these markers with other diagnostic markers as a diagnostic panel. The specific molecular mechanisms of (*Mfn2* and YME1L) have not been fully illustrated so this study tries to discuss the possible mechanisms of these mitochondrial proteins in hepatocarcinogenesis.

Suppressing mitochondrial fusion, thereby elevating fragmentation, leads to increased cellular proliferation and an increase in the mitotic index as mitochondrial fission facilitates the G1/S phase transition of the cell cycle[27]. In agreement with these results, the present experiment revealed that the HCC groups that showed dysregulation of mitochondrial dynamics protein displayed high expression of the tumor proliferation marker ki67 and the cell cycle regulator (cyclin D1). A previous study also showed that *Mfn2* exhibits antiproliferative activity by prompting the Ras-Raf-ERK signaling pathway[28] and Wnt/β-catenin pathway[29]. Loss of YME1L also participated in reducing cell proliferation and altering mitochondrial ultrastructure[30].

Proteins participating in the fission and fusion of the mitochondrial membrane were found to actively contribute to apoptosis stimulation. Although previous studies were indicating that inhibiting mitochondrial fusion can induce apoptosis[31], other studies illustrated the pro-apoptotic role of *Mfn2* as it participates in the regulation of ERK1/2 signalling, which stimulates apoptosis[32]. The *Mfn2* upregulation was also found to have an apoptotic effect in vascular smooth muscle cells[33] or heart muscle cells[34] by suppressing Ras–PI3K–Akt signal pathway. These findings agreed with our study that revealed that apoptosis is inhibited in the HCC groups with altered *Mfn2* and YME1L expression. YME1L was also found to control the accumulation of respiratory chain subunits, which leads to apoptotic resistance[30].

Although alterations in mitochondrial function have been involved in tumorigenesis, few studies have been reported about mitochondrial dynamic roles in metastasis, the major cause of cancer-related mortality, especially in HCC. Our study revealed that the dysregulation of the expression of mitochondrial proteins (*Mfn-2* and YME1L) has been implicated in HCC metastasis by inhibiting the *Timp-3* expression and upregulating the MMP-9 level. Other studies also revealed that silencing of mitofusin proteins caused mitochondrial fragmentation and increased metastasis of other cancer like breast cancer[35]. In thyroid cancer, it was noticed that overexpression of *Mfn2* in cancer cell lines markedly suppressed the cell migration and invasion by modulating the epithelial to mesenchymal transition[36]. Our study also indicates the positive relation between YME1L protein expression and cell proliferation, which participates in increasing invasive behavior of HCC, suggesting that YME1L may potentially increase the tendency of the cancer cell to metastasis. However, there are no previous studies that illustrated its role in tumor cell invasion or metastasis.

Mitochondria regulate metabolic signaling, including reactive oxygen species (ROS). Mitochondrial morphology transitions also were found to control the ROS release[37]. Our study displayed that the HCC groups that revealed multiple fission sites showed more oxidative stress than the control groups. Our findings agreed with previous studies, which illustrated that the fragmented mitochondria observed after Mfn1 knockdown or Drp1 overexpression in various HCC cell lines were related to the overproduction of ROS[38]. On the other hand, Mfn1 knockdown or Drp1 overexpression decreased ROS production as mitochondrial fission-induced redox activation of Akt stimulated Mdm2-dependent ubiquitin-proteasomal degradation of p53 and IKK-dependent NF-κB activation[38]. Few studies demonstrated the role of *Mfn-2* and YME1L in oxidative stress in HCC. However, a previous study illustrated that *Mfn-2* deficiency increases oxidative stress, which participates in insulin resistance[39]. Another study also revealed that inhibition of *Mfn-2* promotes cardiac fibroblast activation through activation of ROS production[40].

Sorafenib, FDA Approved drug, has been used for the treatment of unresectable HCC[37]. Understanding the underlying molecular mechanisms of sorafenib in the treatment of HCC helps in the identification of

patients who could benefit from this therapy. Our study revealed a new target of sorafenib through regulating mitochondrial dynamics as it played a role in regulating the hepatic expression of mitochondrial proteins (MFN-2 and YME1L). Few studies illustrated the effect of sorafenib on mitochondrial dynamics. Our finding disagreed with another study that reported that the treatment with sorafenib induces mitochondrial fragmentation[41]. Our study revealed that the treatment with sorafenib induced mitochondrial fusion, which helped in decreased the tumor cells proliferation, which was illustrated by its role in decreasing the hepatic expression of Ki67 and cell cycle arrest. Sorafenib also increased apoptosis which may be due to its role in increasing the hepatic expression of *Mfn2*, which was previously reported about its role in inducing apoptosis by inhibiting Ras–PI3K–Akt signaling[34]. The treatment with sorafenib in our study also inhibited metastasis and invasion through downregulation of *Timp-3* and MMP-9, which agreed with another previous study[42].

Conclusion

Our study revealed that dysregulation of mitochondrial dynamics represents a key mechanism in liver cancer. Alteration in MFN-2 and YME1L expression in the hepatic tissue are potential diagnostic and prognostic biomarkers for HCC. This study supports the assumption that alterations in the expression of these proteins could be used as predictive tools of outcomes in HCC. These proteins are implicated in tumor cell proliferation and metastasis.

Conflict of interest

All authors declare no Conflict of interest.

References

1 Kim SS, Baek GO, Ahn HR, Sung S, Seo CW, Cho HJ, Nam SW, Cheong JY & Eun JW, Serum small extracellular vesicle-derived LINC00853 as a novel diagnostic marker for early hepatocellular carcinoma. *Mol Oncol*, 14 (2020) 2646.

2 Kirchberger-Tolstik T, Ryabchykov O, Bocklitz T, Dirsch O, Settmacher U, Popp J & Stallmach A, Nondestructive molecular imaging by Raman spectroscopy vs. marker detection by MALDI IMS for an early diagnosis of HCC. *Analyst*, 146 (2021) 1239.

3 Shmatko A, Ghaffari Laleh N, Gerstung M & Kather JN, Artificial intelligence in histopathology: enhancing cancer research and clinical oncology. *Nat Cancer*, 3 (2022) 1026.

4 Dasgupta A, Chen KH, Wu D, Hoskin V, Mewburn J, Lima PD, Parlow LR, Hindmarch CC, Martin A & Sykes EA, An epigenetic increase in mitochondrial fission by MiD49 and MiD51 regulates the cell cycle in cancer: Diagnostic and therapeutic implications. *FASEB J*, 34 (2020) 5106.

5 Mohanraj K, Nowicka U & Chacinska A, Mitochondrial control of cellular protein homeostasis. *Biochem J*, 477 (2020) 3033.

6 Rodrigues T &Ferraz LS, Therapeutic potential of targeting mitochondrial dynamics in cancer. *Biochem Pharmacol*, 182 (2020) 114282.

7 Abdel-Hamid NM, Abass SA, Eldomany RA, Abdel-Kareem MA & Zakaria S, Dual regulating of mitochondrial fusion and Timp-3 by leflunomide and diallyl disulfide combination suppresses diethylnitrosamine-induced hepatocellular tumorigenesis in rats. *Life Sci*, 294 (2022) 120369.

8 Giacomello M, Pyakurel A, Glytsou C & Scorrano L, The cell biology of mitochondrial membrane dynamics. *Nat Rev Mol Cell Biol*, 21 (2020) 204.

9 Xue R, Yang J, Jia L, Zhu X, Wu J, Zhu Y & Meng Q, Mitofusin2, as a Protective Target in the Liver, Controls the Balance of Apoptosis and Autophagy in Acute-on-Chronic Liver Failure. *Front Pharmacol*, 10 (2019).

10 Purohit PK, Edwards R, Tokatlidis K & Saini N, MiR-195 regulates mitochondrial function by targeting mitofusin-2 in breast cancer cells. *RNA Biol*, 16 (2019) 918.

11 Li J, Gao JZ, Du JL & Wei LX, Prognostic and clinicopathological significance of glypican-3 overexpression in hepatocellular carcinoma: a meta-analysis. *World J Gastroenterol*, 20 (2014) 6336.

12 Tan Y, Xia F, Li L, Peng X, Liu W, Zhang Y, Fang H, Zeng Z & Chen Z, Novel Insights into the Molecular Features and Regulatory Mechanisms of Mitochondrial Dynamic Disorder in the Pathogenesis of Cardiovascular Disease. *Oxid Med Cell Longev*, 2021 (2021) 6669075.

13 Cesnekova J, Rodinova M, Hansikova H, Zeman J & Stiburek L, Loss of Mitochondrial AAA Proteases AFG3L2 and YME1L Impairs Mitochondrial Structure and Respiratory Chain Biogenesis. *Int J Mol Sci*, 19 (2018) 3930.

14 Ohba Y, MacVicar T & Langer T, Regulation of mitochondrial plasticity by the i-AAA protease YME1L. *Biol Chem*, 401 (2020) 877.

15 Jilkova ZM, Kuyucu AZ, Kurma K, Ahmad Pour ST, Roth GS, Abbadessa G, Yu Y, Schwartz B, Sturm N, Marche PN, Hainaut P & Decaens T, Combination of AKT inhibitor ARQ 092 and sorafenib potentiates inhibition of tumor progression in cirrhotic rat model of hepatocellular carcinoma. *Oncotarget*, 9 (2018) 11145.

16 Reitman S &Frankel S, A colorimetric method for the determination of serum glutamic oxalacetic and glutamic pyruvic transaminases. *Am J Clin Pathol*, 28 (1957) 56.

17 Beutler E, Duron O & Kelly BM, Improved method for the determination of blood glutathione. *J Lab Clin Med*, 61 (1963) 882.

18 Ohkawa H, Ohishi N & Yagi K, Assay for lipid peroxides in animal tissues by thiobarbituric acid reaction. *Anal Biochem*, 95 (1979) 351.

19 Kang S, Byun J, Son SM & Mook-Jung I, Thrombospondin-1 protects against Aβ-induced mitochondrial fragmentation and dysfunction in hippocampal cells. *Cell Death Discov*, 4 (2018) 1.

20 Ghosh S, Bhowmik S, Majumdar S, Goswami A, Chakraborty J, Gupta S, Aggarwal S, Ray S, Chatterjee R & Bhattacharyya S, The exosome encapsulated microRNAs as circulating diagnostic marker for hepatocellular carcinoma with low alpha-fetoprotein. *Int J Cancer*, 147 (2020) 2934.

21 Rashed WM, Kandeil MAM, Mahmoud MO & Ezzat S, Hepatocellular Carcinoma (HCC) in Egypt: A comprehensive overview. *J Egypt Natl Canc Inst*, 32 (2020) 5.

22 Lin XH, Qiu BQ, Ma M, Zhang R, Hsu SJ, Liu HH, Chen J, Gao D-M, Cui J-F & Ren Z-G, Suppressing DRP1-mediated mitochondrial fission and mitophagy increases mitochondrial apoptosis of hepatocellular carcinoma cells in the setting of hypoxia. *Oncogenesis*, 9 (2020) 1.

23 Gao S & Hu J, Mitochondrial fusion: the machineries in and out. *Trends Cell Biol*, 31 (2021) 62.

24 Ge Y, Shi X, Boopathy S, McDonald J, Smith AW & Chao LH, Two forms of Opa1 cooperate to complete fusion of the mitochondrial inner-membrane. *Elife*, 9 (2020) e50973.

25 Bao D, Zhao J, Zhou X, Yang Q, Chen Y, Zhu J, Yuan P, Yang J, Qin T, Wan S & Xing J, Mitochondrial fission-induced mtDNA stress promotes tumor-associated macrophage infiltration and HCC progression. *Oncogene*, 38 (2019) 5007.

26 Wang X, Liu Y, Sun J, Gong W, Sun P, Kong X, Yang M & Zhang W, Mitofusin-2 acts as biomarker for predicting poor prognosis in hepatitis B virus related hepatocellular carcinoma. *Infect Agent Cancer*, 13 (2018) 36.

27 Zhan L, Cao H, Wang G, Lyu Y, Sun X, An J, Wu Z, Huang Q, Liu B & Xing J, Drp1-mediated mitochondrial fission promotes cell proliferation through crosstalk of p53 and NF-κB pathways in hepatocellular carcinoma. *Oncotarget*, 7 (2016) 65001.

28 Chen KH, Dasgupta A, Ding J, Indig FE, Ghosh P & Longo DL, Role of mitofusin 2 (Mfn2) in controlling cellular proliferation. *FASEB J*, 28 (2014) 382.

29 Pang G, Xie Q & Yao J, Mitofusin 2 inhibits bladder cancer cell proliferation and invasion via the Wnt/β-catenin pathway. *Oncol Lett*, 18 (2019) 2434.

30 Stiburek L, Cesnekova J, Kostkova O, Fornuskova D, Vinsova K, Wenchich L, Houstek J & Zeman J, YME1L controls the accumulation of respiratory chain subunits and is required for apoptotic resistance, cristae morphogenesis, and cell proliferation. *Mol Biol Cell*, 23 (2012) 1010.

31 Sugioka R, Shimizu S & Tsujimoto Y, Fzo1, a protein involved in mitochondrial fusion, inhibits apoptosis. *J Biol Chem*, 279 (2004) 52726.

32 Cheung EC & Slack RS, Emerging role for ERK as a key regulator of neuronal apoptosis. *Sci STKE*, 2004 (2004) 45.

33 Guo X, Chen K-H, Guo Y, Liao H, Tang J & Xiao R-P, Mitofusin 2 triggers vascular smooth muscle cell apoptosis via mitochondrial death pathway. *Circ Res*, 101 (2007) 1113.

34 Shen T, Zheng M, Cao C, Chen C, Tang J, Zhang W, Cheng H, Chen KH & Xiao RP, Mitofusin-2 is a major determinant of oxidative stress-mediated heart muscle cell apoptosis. *J Biol Chem*, 282 (2007) 23354.

35 Zhao J, Zhang J, Yu M, Xie Y, Huang Y, Wolff DW, Abel PW & Tu Y, Mitochondrial dynamics regulates migration and invasion of breast cancer cells. *Oncogene*, 32 (2013) 4814.

36 You M-H, Jeon MJ, Kim Sr, Lee WK, Cheng SY, Jang G, Kim TY, Kim WB, Shong YK & Kim WG, Mitofusin-2 modulates the epithelial to mesenchymal transition in thyroid cancer progression. *Sci Rep*, 11 (2021) 2054.

37 Nair A, Reece K, Donoghue MB, Yuan W, Rodriguez L, Keegan P & Pazdur R, FDA supplemental approval summary: lenvatinib for the treatment of unresectable hepatocellular carcinoma. *Oncologist*, 26 (2021) e484.

38 Huang Q, Zhan L, Cao H, Li J, Lyu Y, Guo X, Zhang J, Ji L, Ren T, An J, Liu B, Nie Y & Xing J, Increased mitochondrial fission promotes autophagy and hepatocellular carcinoma cell survival through the ROS-modulated coordinated regulation of the NFKB and TP53 pathways. *Autophagy*, 12 (2016) 999.

39 Nie Q, Wang C, Song G, Ma H, Kong D, Zhang X, Gan K & Tang Y, Mitofusin 2 deficiency leads to oxidative stress that contributes to insulin resistance in rat skeletal muscle cells. *Mol Biol Rep*, 41 (2014) 6975.

40 Xin Y, Wu W, Qu J, Wang X, Lei S, Yuan L & Liu X, Inhibition of mitofusin-2 promotes cardiac fibroblast activation *via* the PERK/ATF4 pathway and reactive oxygen species. *Oxid Med Cell Longev*, 2019 (2019) 3649808.

41 Zhao X, Tian C, Puszyk WM, Ogunwobi OO, Cao M, Wang T, Cabrera R, Nelson DR & Liu C, OPA1 downregulation is involved in sorafenib-induced apoptosis in hepatocellular carcinoma. *Lab Invest*, 93 (2013) 8.

42 He XX, Shi LL, Qiu MJ, Li QT, Wang MM, Xiong ZF & Yang SL, Molecularly targeted anti-cancer drugs inhibit the invasion and metastasis of hepatocellular carcinoma by regulating the expression of MMP and TIMP gene families. *Biochem Biophys Res Commun*, 504 (2018) 878.